

# Evolution of the metal content of the intra-cluster medium with hydrodynamical simulations

D. Fabjan<sup>1,2,3</sup>, L. Tornatore<sup>1,2,3</sup>, S. Borgani<sup>1,2,3</sup>, A. Saro<sup>1,3</sup> & K. Dolag<sup>4</sup>

<sup>1</sup> *Dipartimento di Astronomia dell'Università di Trieste, via Tiepolo 11, I-34131 Trieste, Italy (fabjan,borgani,tornatore,saro@oats.inaf.it)*

<sup>2</sup> *INAF – Istituto Nazionale di Astrofisica, via Tiepolo 11, I-34131 Trieste, Italy*

<sup>3</sup> *INFN – Istituto Nazionale di Fisica Nucleare, Trieste, Italy*

<sup>4</sup> *Max-Planck-Institut für Astrophysik, Karl-Schwarzschild Strasse 1, Garching bei München, Germany (kdolag@mpa-garching.mpg.de)*

24 October 2018

## ABSTRACT

We present a comparison between simulation results and X-ray observational data on the evolution of the metallicity of the intra-cluster medium (ICM). The simulations of galaxy clusters have been carried out using a version of the TREEPM-SPH GADGET-2 code that includes a detailed model of chemical evolution, by assuming three different shapes for the stellar initial mass function (IMF). Besides the Salpeter (1955) IMF, we used also the IMF proposed by Kroupa (2001) and the top-heavier IMF by Arimoto & Yoshii (1987). We find that simulations predict significant radial gradients of the Iron abundance,  $Z_{\text{Fe}}$ , which extend over the whole cluster virialized region. Using the Salpeter IMF, the profiles of  $Z_{\text{Fe}}$  have an amplitude which is in a reasonable agreement with *Chandra* observations within  $0.2R_{500}$ . At larger radii, we do not detect any flattening of the metallicity profiles.

As for the evolution of the ICM metal abundance out to  $z = 1$ , it turns out that the results based on the Salpeter IMF agree with observations. We find that the evolution of  $Z_{\text{Fe}}$  in simulations is determined by the combined action of (i) the sinking of already enriched gas, (ii) the ongoing metal production in galaxies and (iii) the locking of ICM metals in newborn stars. As a result, rather than suppressing the metallicity evolution, stopping star formation at  $z = 1$  has the effect of producing an even too fast evolution of the emission-weighted ICM metallicity, with too high values of  $Z_{\text{Fe}}$  at low redshift within  $0.2R_{200}$ . Finally, we compare simulations with the observed rate of type-Ia supernovae per unit B-band luminosity ( $\text{Sn}U_B$ ). We find that our simulated clusters do not reproduce the decreasing trend of  $\text{Sn}U_B$  at low redshift, unless star formation is truncated at  $z = 1$ .

**Key words:** Cosmology: Theory – Methods: Numerical – X-Rays: Galaxies: Clusters – Galaxies: Abundances – Galaxies: Intergalactic Medium

## 1 INTRODUCTION

The high quality X-ray observations of galaxy clusters from the current generation of X-ray satellites are allowing now to trace in detail the pattern of the metal enrichment of the intra-cluster medium of galaxies (e.g., Mushotzky 2004; Werner et al. 2008, for reviews). In turn, this information is inextricably linked to the history of formation and evolution of the galaxy population as observed in the optical/near-IR band (e.g., Renzini 2004, and references therein). A number of independent observations have established that significant radial gradients of the Iron abundance are present in the central regions,  $R \lesssim 0.1R_{500}$ , of relaxed clusters and groups (e.g., De Grandi et al. 2004; Vikhlinin et al. 2005; Rasmussen & Ponman 2007), with enhancement of the metallicity associated to the brightest cluster galaxies (BCGs), while no evidence has been found that these gradients extend at larger cluster-

centric distances (e.g., Snowden et al. 2008). Furthermore, deep exposures with the *Chandra* and *XMM-Newton* satellites have now opened the possibility of tracing the evolution of the ICM metal content within the central regions out to the largest redshifts,  $z \simeq 1.3$ , where clusters have been identified so far. Balestra et al. (2007) and Maughan et al. (2008) have analysed fairly large samples of distant clusters, extracted from the *Chandra* archive and found that the metallicity of the ICM within the central cluster regions has increased by about 50 per cent since  $z \simeq 1$ .

This positive evolution of the ICM metallicity in the central cluster regions is apparently in contradiction with the lack of significant star formation at low redshift (e.g., Rafferty et al. 2006). Based on a phenomenological approach, Ettori (2005) showed that the evolution of the ICM metallicity is in line with the expectations from the observed cosmic rates of supernova (Sn) explosions and of

star formation. Loewenstein (2006) combined observations of the evolution of the ICM metallicity with data on the Sn rates and star formation rates to infer the relative role played by type Ia and II Sn (SnIa and SnII hereafter).

A different approach was pursued by other authors, which considered gas–dynamical mechanisms that at relatively low redshift are responsible for redistributing previously produced metals. For instance, Cora et al. (2008) suggested that clumps of low–entropy highly enriched gas may sink in the central cluster regions, thereby leading to an increase of the observed emission–weighted metallicity. For instance, ram–pressure stripping of the interstellar medium (ISM) of merging galaxies has been suggested as a mechanism to pollute at relatively low redshift a metal–poor ICM with highly enriched gas (e.g., Domainko et al. 2006, and references therein), while causing a morphological transformation of cluster galaxies (e.g., Calura et al. 2007; Roediger & Brüggen 2007). Although possible evidences of ram–pressure stripping of cluster galaxies have been detected (e.g., Chung et al. 2007) the question remains as to whether this mechanism dominates the evolution of the ICM enrichment. Indeed, since ram pressure is expected to be more efficient in high–temperature clusters, one expects an increasing trend of metallicity with ICM temperature (e.g., Renzini 1997). If any, observations suggest that hotter systems have a relatively lower metallicity (e.g., Baumgartner et al. 2005), thus suggesting that ram–pressure stripping is not the dominant process in enriching the ICM.

It is clear that understanding the history of the ICM enrichment in cosmological context, during the cluster hierarchical build up, requires describing in detail the gasdynamics related to the merging processes, while including a self–consistent treatment of star formation and chemical evolution. In this context, cosmological hydrodynamical simulations offer a unique means to capture in full detail the complexity of these processes (e.g., Valdarnini 2003; Tornatore et al. 2004; Romeo et al. 2006; Tornatore et al. 2007, see Borgani et al. 2008, for a recent review). In their most advanced versions, chemo–dynamical simulation codes treat the production of different metal species, released by different stellar populations by resorting to detailed stellar yields, also accounting for the mass–dependent stellar lifetimes.

In this paper we will present results on the ICM metal abundance from cosmological simulations of galaxy clusters, using the chemo–dynamical version of the GADGET-2 code (Springel et al. 2001; Springel 2005), which has been recently presented by Tornatore et al. (2007) (T07 hereafter). We will compare the simulations with observational results on the Iron abundance profiles,  $Z_{\text{Fe}}$ , of nearby clusters, on the evolution of the ICM metallicity and on the SnIa rates. This comparison will be performed with the aim of shading light on the relative role played by star formation, feedback processes and gas dynamics in determining the cosmic history of metal enrichment.

The plan of the paper is as follows. In Section 2 we review our implementation of chemical evolution in the GADGET-2 code and present the main characteristics of the cluster simulations. Section 3 will be devoted to the comparison between simulation results and observations. After comparing the profiles of the Iron abundance, we will concentrate on the evolution of the ICM metallicity. We will then compare observations and simulation predictions on the rate of SnIa. We will draw our conclusions in Section 4.

All values of Iron abundance that we will quote in the following are scaled to the solar abundance value by Grevesse & Sauval (1998).

## 2 THE SIMULATIONS

In this letter we present a set of simulations of four massive isolated clusters, which have been identified in a Dark–Matter only simulation having a box size  $479 h^{-1} \text{Mpc}$  (Yoshida et al. 2001), performed for a flat  $\Lambda$ CDM cosmological model with  $\Omega_m = 0.3$ ,  $h_{100} = 0.7$ ,  $\sigma_8 = 0.9$  and  $\Omega_b = 0.04$ . The four extracted Lagrangian regions, centred on these clusters with virial masses<sup>1</sup> in the range  $M_{\text{vir}} = 1.0\text{--}2.3 \times 10^{15} h^{-1} M_{\odot}$ , have been resimulated using the Zoomed Initial Condition (ZIC) technique by Tormen et al. (1997), which allows one to increase force and mass resolution in the regions of interest. The high–resolution DM particles have mass  $m_{DM} = 1.13 \times 10^9 h^{-1} M_{\odot}$ , and the barionic particles have been added with a mass  $m_{gas} = 1.7 \times 10^8 h^{-1} M_{\odot}$  in order to reproduce the assumed cosmic barionic fraction. The basic characteristics of the simulated clusters are summarized in Table 1.

The simulations are performed using the hydrodynamical Tree-SPH code GADGET-2 (Springel 2005) with the implementation of chemical enrichment by T07. The Plummer–equivalent softening length for gravitational force is set to  $\epsilon = 5 h^{-1} \text{kpc}$  in physical units from  $z = 2$  to  $z = 0$ , while at higher redshifts is  $\epsilon = 15 h^{-1} \text{kpc}$  in comoving units. The simulations include heating from a uniform time–dependent UV background (Haardt & Madau 1996) and metallicity–dependent radiative cooling based on the tables by Sutherland & Dopita (1993) for an optically thin plasma. The process of star formation (SF hereafter) is described by the sub–resolution multiphase model by Springel & Hernquist (2003), for which the density threshold for the onset of SF is set to  $n_H = 0.1 \text{cm}^{-3}$ .

While the relevant features of the chemical evolution model are described here below, we address the reader to T07 for a more detailed description. Metals are produced by SnII, SnIa and intermediate and low–mass stars (ILMS hereafter), with only SnIa and SnII providing energy feedback. We assume SnII to arise from stars having mass above  $8M_{\odot}$ . As for the SnIa, we assume their progenitors to be binary systems, whose total mass lies in the range  $(3\text{--}16)M_{\odot}$ . Metals and energy are released by stars of different mass by properly accounting for mass–dependent lifetimes. In this work we assume the lifetime function proposed by Padovani & Matteucci (1993). We adopt the metallicity–dependent stellar yields by Woosley & Weaver (1995) for SnII, the yields by van den Hoek & Groenewegen (1997) for the ILMS and by Thielemann et al. (2003) for SnIa. The version of the code used for the simulations presented here allowed us to follow H, He, C, N, O, Mg, Si and Fe. Once produced by a star particle, metals are then spread to the surrounding gas particles by using the B-spline kernel with weights computed over 64 neighbours and taken to be proportional to the volume of each particle. T07 verified with detailed tests that the final results on the pattern of chemical enrichment are rather insensitive to the weighting scheme (kernel shape and number of neighbours) used to spread metals.

Our simulations include the kinetic feedback model implemented by Springel & Hernquist (2003). According to this scheme,

<sup>1</sup> We define the virial mass  $M_{\text{vir}}$  as the mass contained within the virial radius  $R_{\text{vir}}$ . This is defined as the radius within which the average density  $\rho_{\text{vir}}$  is that predicted by the spherical collapse model (for the cosmology assumed in our simulations,  $\rho_{\text{vir}} \simeq 100\rho_c$ , with  $\rho_c$  the critical cosmic matter density). More in general, we define  $R_{\Delta}$  to be the radius at which the density is  $\Delta$  times the critical density  $\rho_c$ . Physical quantities with subscript  $\Delta$  are computed within  $R_{\Delta}$ .

SnII explosions trigger galactic winds, whose mass upload rate is assumed to be proportional to the star formation rate,  $\dot{M}_W = \eta \dot{M}_*$ . Therefore, fixing the parameter  $\eta$  and the wind velocity  $v_W$  amounts to fix the total energy carried by the winds. Our choice of  $\eta = 3$  and  $v_W = 500 \text{ km s}^{-1}$  corresponds to assume, for the initial mass function (IMF) by Salpeter (1955), with SnII releasing  $10^{51}$  ergs each, nearly unity efficiency in powering galactic outflows.

In our comparison with observational data, we will first explore the effect of changing the IMF. We use the IMF by Salpeter (1955) and that by Arimoto & Yoshii (1987), for which the number  $N$  of stars per unit mass interval is defined as  $\varphi(m) \propto dN/dm \propto m^{-(1+x)}$ , with  $x = 1.35$  and  $x = 0.95$  respectively. Furthermore, we also use the multi-slope IMF proposed by Kroupa (2001) with  $x = -0.7, 0.3$  and  $1.3$  respectively for  $m \leq 0.08 M_\odot$ ,  $0.08 \leq m < 0.5 M_\odot$  and  $m \geq 0.5 M_\odot$ . Simulations based on the Salpeter IMF have been run for the four clusters, while only simulations of the g51 halo have been carried out for the other two choices of the IMF. In the following, we label the runs that use the Salpeter, Arimoto–Yoshii and Kroupa IMFs with *Sal*, *AY* and *Kr* respectively.

An important parameter entering in the model of chemical evolution is the fraction  $A$  of stars, in the mass range  $0.8\text{--}8 M_\odot$ , belonging to binary systems which explodes as SnIa in the single-degenerate scenario (Greggio & Renzini 1983; Matteucci & Greggio 1986). For our reference runs we will use  $A = 0.1$ , as suggested by Matteucci & Gibson (1995) to reproduce the observed ICM metallicity (see also Portinari et al. 2004). As we shall discuss in the following, the simulation with the *AY* IMF tends to overproduce Iron. In the attempt to overcome this problem, we also carried out a run with the *AY* IMF using also  $A = 0.05$ .

Simulations of galaxy clusters, which include the scheme of feedback adopted here, are already known to produce an excess of low-redshift star formation, mostly associated with the BCG (e.g., Romeo et al. 2005; Saro et al. 2006). This recent star formation is expected to significantly affect the history of the ICM enrichment. From one hand, it should provide an excess of recent metal production, thus possibly enhancing the enrichment at small cluster-centric radii. On the other hand, a recent star formation is also expected to lock back in the stellar phase a significant amount of highly enriched gas, which has shorter cooling time, thus leaving in the hot ICM only relatively metal-poorer gas. In order to quantify the effect of recent star formation of the ICM enrichment history, we have also simulated the *Sal* version of the g51 cluster by switching off radiative cooling and star formation below  $z = 1$ , considering both the case in which already formed stars keep producing metals with the appropriate lifetimes (CS run) and the case in which also the metal production is stopped at the same redshift (CMS run). While this prescription of suppressing low-redshift star formation and metal production is admittedly oversimplified, it allows us to address the following questions: (i) to what extent the SF excess in simulations affects the enrichment evolution of the ICM? (ii) which is the role of gas-dynamical processes in redistributing at relatively low redshift the metals that have been produced at earlier epochs?

### 3 RESULTS AND DISCUSSION

#### 3.1 Metallicity profiles of nearby clusters

The radial profiles of the metal abundance provide a very important record of the chemical enrichment process in galaxy clusters.

Cluster	$M_{\text{vir}}$	$R_{\text{vir}}$	$T_{\text{vir}}^{\text{sl}}$
g1	1.49	2.33	7.90
g8	2.24	2.67	9.47
g72	1.34	2.26	6.23
g51	1.30	2.23	7.19

**Table 1.** Characteristics of the simulated clusters at  $z = 0$ . Column 1: cluster name; column 2: virial mass (units of  $10^{15} h^{-1} M_\odot$ ); column 3: virial radius (units of  $h^{-1} \text{Mpc}$ ); column 4: spectroscopic-like temperature within  $R_{\text{vir}}$  (keV, see Mazzotta et al. (2004), for its definition).

Indeed, they are determined by the distribution of cluster galaxies, where most of the metals are produced, by the mechanisms responsible for their transport and diffusion from the star-forming regions (i.e., galactic ejecta, ram-pressure and viscous stripping, etc.) and by other gas-dynamical processes which redistribute them on larger scales (e.g. turbulence and sinking of enriched low-entropy gas). Here we compare the profiles of the Iron abundance of simulated galaxy clusters at  $z = 0$  with the observational results from *Chandra* data of a sample of nearby relaxed clusters analysed by Vikhlinin et al. (2005).

In Figure 1 we compare the profiles of  $Z_{\text{Fe}}$  from our simulated clusters with the observed profiles of 8 clusters having temperature above 3 keV (see Table 1 in Vikhlinin et al. 2005). We point out that the analysis of Vikhlinin et al. (2005) provided information on the total ICM metallicity, i.e. without distinguishing the contribution from different chemical species. However, at the typical temperatures of these clusters and for the typical energy range where the spectral analysis was performed (0.6–10 keV; see Vikhlinin et al. 2005), this observed metallicity is largely dominated by Iron. We want to stress the fact that the simulated clusters are dynamically relaxed (with the last major merger undergone before  $z = 0.5$ ) and therefore suitable for the comparison with this set of observed clusters.

As shown in the left panel of Fig.1, the simulations based on a Salpeter (1955) IMF produce profiles which are in reasonable agreement with observations. The scatter among the four simulated clusters is quite small, with some increase in the central regions,  $R \lesssim 0.1 R_{500}$ . Although observations seem to have a larger scatter, it is not clear how much observational uncertainties contribute to it. Changing the IMF (right panel of Fig. 1) clearly turns into a change of the overall amount of the Iron abundance at all radii, with both the Kroupa and the *AY* IMFs producing too high profiles. The larger amount of Iron found for these two IMFs is due to the fact that, once normalized, they both predict a larger number of supernovae contributing to the Iron production, with respect to the Salpeter one.

Besides producing more SnII, the *AY* and *Kr* IMFs also produce a larger number of SnIa, since there is a significant overlap between the mass range relevant for SnIa and the mass range where these two IMFs are higher than the Salpeter one.

As for the relative roles of SnIa, SnII and ILSM in the ICM enrichment, we verified that SnIa contribute for about 70 per cent of the Iron contained in the diffuse medium within  $R_{500}$  for the Salpeter IMF. This fraction decreases to about 65 per cent for the Kroupa IMF and to about 55 per cent for the Arimoto–Yoshii IMF. Since SnIa provide a major contribution to the Iron production, our results are quite sensitive to the choice of the fraction  $A$  of stars in binary systems. As a matter of fact, this fraction can be considered as a free parameter in a model of chemical evolution. Following a phenomenological approach, for each choice of the IMF its

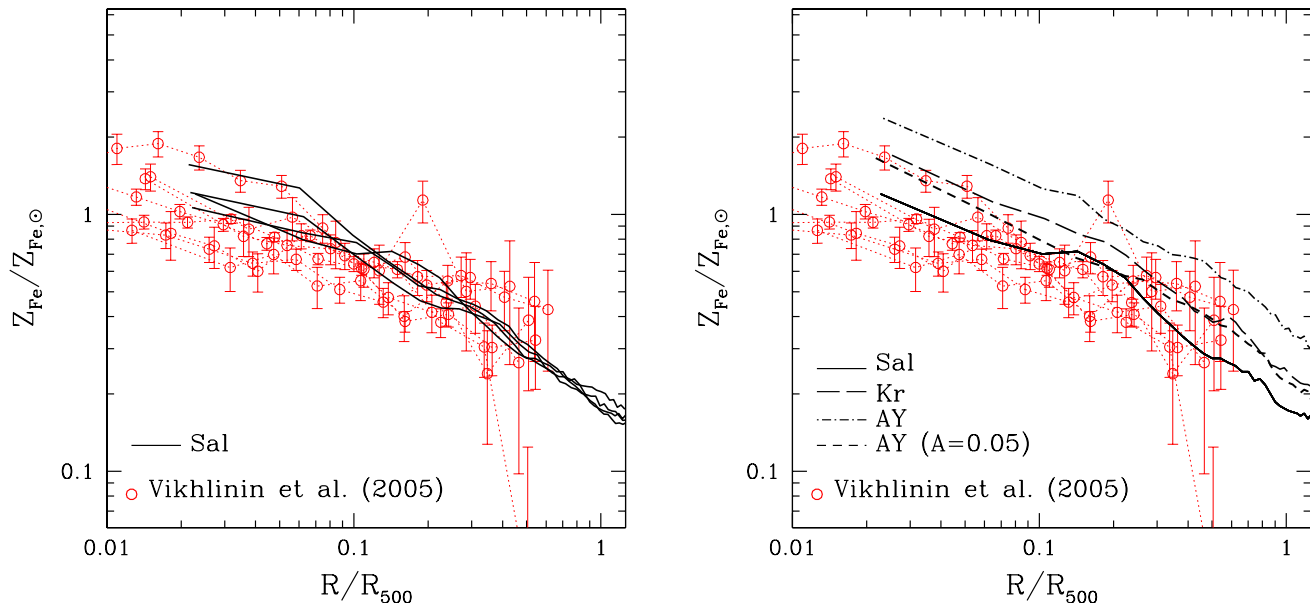


**Figure 1.** The Iron abundance profiles of simulated clusters at  $z = 0$  compared to the Chandra observed profiles for 8 nearby clusters with  $T > 3$  keV (Vikhlinin et al. 2005) (open circles with errorbars). In the left panel the solid curves correspond to the four clusters simulated using the Salpeter (1955) IMF. The right panel compares the results of the g51 cluster simulated using the IMF by Salpeter (1955) (solid), by Arimoto & Yoshii (1987) with two different values for the fraction of binary stars ( $A = 0.1$ : dot-dashed;  $A = 0.05$ : short dashed) and by Kroupa (2001) (long dashed).

value is determined by the requirement of reproducing some observational data. In our case, we note that decreasing  $A$  from 0.1 to 0.05 induces a significant decrease of the  $Z_{\text{Fe}}$  profile. This sort of degeneracy between the IMF shape and the fraction of binary stars can be broken by looking at the relative abundance of  $\alpha$  elements with respect to Iron. For instance, since Oxygen is essentially produced by SnII, we expect a top-heavier IMF to provide values of O/Fe higher than for a top-lighter IMF. If we suppress the number of SnIa for the top-heavier IMF, by decreasing the value of  $A$ , we further increase the O/Fe ratio, thus allowing to distinguish this case from that of a top-lighter IMF with a higher  $A$ . We deserve a forthcoming paper to a detailed comparison of simulations with observations of relative abundances for nearby clusters.

The runs with the Salpeter IMF provide results in closer agreement with the Chandra data, although in all cases the profiles of the simulated clusters are somewhat steeper than the observed ones, with negative gradients extending at least out  $R_{500}$  and beyond. This result is at variance with the recent claim by Snowden et al. (2008) who found no evidence for the presence of metallicity gradients at scales  $\gtrsim 0.1R_{500}$  from the analysis of a catalog of 70 clusters observed with XMM-Newton. In the next section we will compare simulated and observed results on the evolution of the ICM metallicity at small radii, where the simulated and the observed metallicity gradients are in reasonable agreement. If confirmed by independent analyses, the lack of abundance gradients at relatively large radii will provide a non-trivial constraint for chemo-dynamical models of the ICM enrichment.

Limited numerical resolution could lead to an underestimate of high-redshift enrichment from a pristine population of relatively small under-resolved galaxies. This high- $z$  enrichment should be rather uniform and, therefore, should soften the metallicity gradients. Indeed, T07 found that increasing resolution provides pro-

gressively shallower metallicity profiles. However, the effect is visible only at radii  $\gtrsim 0.5R_{500}$ , while being negligible at smaller radii, which are dominated by the star formation associated to the BCG. Another possibility to soften metallicity profiles can be provided by AGN feedback. For instance, Bhattacharya et al. (2007) analysed cosmological simulations of galaxy groups, which include the effect of energy feedback from gas accretion onto black holes. They found that the effect of this feedback is to redistribute the hot gas, driving it from the inner regions, where it should be more enriched, to the outer part of the halo, and to lower the star formation in the inner region. Sijacki & Springel (2006a) used a similar feedback scheme, in which energy is used to trigger the formation of high entropy bubbles. These bubbles rise buoyantly in the ICM, giving rise to a redistribution of the central metal-enriched gas (see also Roediger et al. 2007). Clearly, in this case the request is that the redistribution of metals should not be so efficient as to destroy the metallicity gradients in the central cluster regions (e.g., Böhringer et al. 2004).

### 3.2 Evolution of the ICM metallicity

In this Section we compare the simulation predictions on the evolution of the ICM metallicity with the observational results by Balestra et al. (2007). These authors analysed *Chandra* observations of 56 clusters at  $z > 0.3$  (with the addition of XMM-Newton observations for clusters at  $z > 1$ ) having temperatures above 3 keV. They measured the metallicity in the central regions, with a typical extraction radius of  $0.15\text{--}0.3 R_{180}$ , chosen object-by-object so as to maximize the signal-to-noise ratio (see also Maughan et al. 2008, for a similar analysis). For the low-redshift reference value, Balestra et al. (2007) combined this set of distant clusters with a mix of cool-core and non cool-core clusters at lower redshift. They

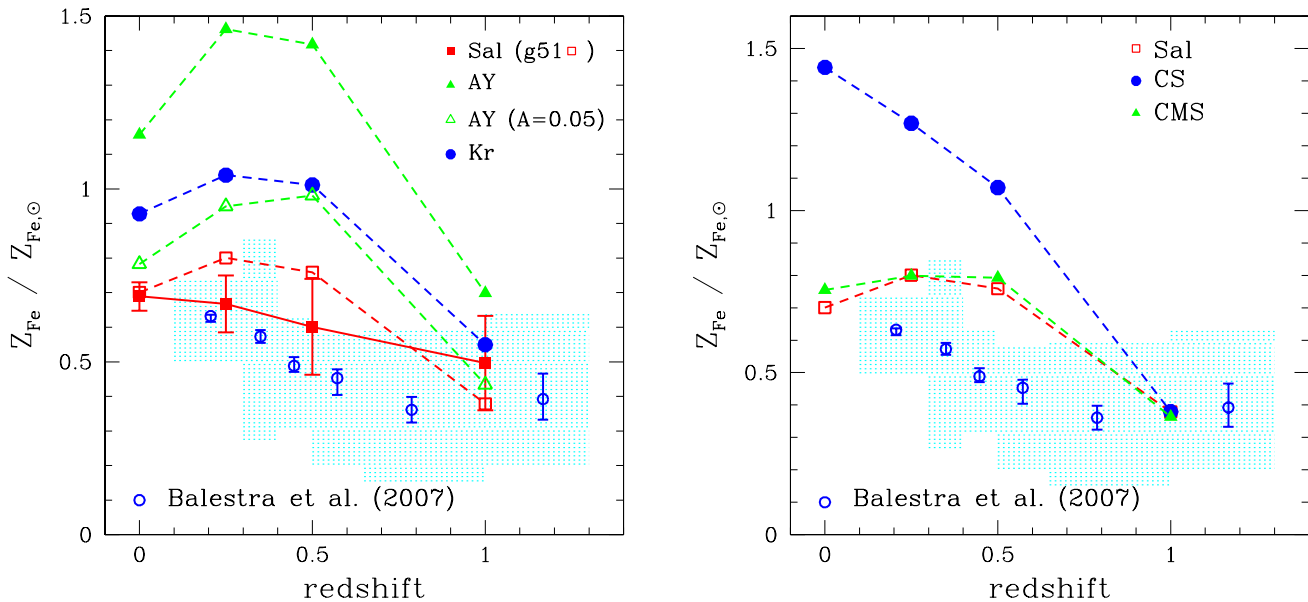


**Figure 2.** The comparison between observations and simulations for the evolution of the Iron abundance,  $Z_{\text{Fe}}$ . Observational results from Balestra et al. (2007) are shown with open circles, with errorbars corresponding to the  $1\sigma$  uncertainty in the combined spectral fit performed for all the clusters falling within each redshift bin. The shaded area is the r.m.s. scatter among the measured metallicities within the same redshift intervals. Left panel: the dependence of the simulation results on the stellar IMF. The filled squares show the average over the simulated clusters, assuming a Salpeter (1955) IMF (*Sal*), with errorbars indicating the r.m.s. scatter over the four objects. For the g51 cluster only, the open squares are for the run with Salpeter (1955) IMF, the filled and open triangles are for the Arimoto & Yoshii (1987) IMF (*AY*) with  $A = 0.1$  and  $A = 0.05$  for the binary fractions, respectively, while the filled circles are for the run with the Kroupa (2001) IMF (*Kr*). Right panel: the effect of stopping star formation and metal production at low redshift on the evolution of  $Z_{\text{Fe}}$  for the g51 cluster, using the Salpeter (1955) IMF. Results for the reference (*Sal*) run are shown with the open squares. The filled circles are for the simulation with radiative cooling and star formation stopped at  $z = 1$  (*CS*), while the filled triangles are for the run in which also the metal production is turned off at  $z = 1$  (*CMS*).

also pointed out that the observed decrease of  $Z_{\text{Fe}}$  with redshift is not induced by a decrease of the fraction of cool-core clusters in the past. Therefore, we expect that no significant bias is introduced when comparing the observed evolution with that traced by our set of relaxed simulated clusters. Since it is quite difficult to define a common extraction radius for the observed clusters, we decided to adopt a value of  $0.2R_{180}$  in the analysis of the simulated clusters. We verified that our conclusions are left unchanged by varying this radius in the range  $0.15\text{--}0.3 R_{180}$ .

In the left panel of Figure 2 we compare the observational results by Balestra et al. (2007) with the predictions of our simulations for different choices of the IMF. Observations and simulations are compared here by using the emission-weighted definition of metallicity, with emissivity of each gas particle computed in the 0.5–10 keV energy band. In principle, this comparison would require extracting synthetic spectra from the simulated clusters and then measure the metallicity by fitting these spectra to a single-temperature and single-metallicity plasma models, as done in the analysis of observational data. An analysis of this type has been recently presented by Rasia et al. (2007) and showed that, at least for Iron, the emission-weighted estimator gives results quite close (within about 10 per cent) to those obtained from the spectral-fitting analysis.

Interestingly, we note in all simulations a significant increase of metallicity in the cluster central regions below redshift unity. The runs based on the *Sal* IMF provide results close to observations. On the contrary both the *Kr* and the *AY* IMFs predict too high

abundances for the g51 cluster at all redshifts, with a very strong evolution at  $z \gtrsim 0.5$  (we note that g51 is the cluster with the highest metallicity at  $z = 0.25$  and  $0.5$ , among the four simulated objects). This higher abundance for the *AY* and *Kr* IMFs is in line with the correspondingly higher profiles found at  $z = 0$  (see Fig. 1). Again, decreasing the binary fraction in the *AY* run to  $A = 0.05$  causes a significant decrease of the Iron abundance at all redshifts.

At lower redshifts,  $z > 0.5$ , g51 shows a slower evolution, even followed by an inversion below  $z \simeq 0.25$ . The reason for this inversion lies in the quiet accretion history of this clusters below  $z = 0.5$ . Since no highly enriched gas clumps, associated to major merger event, reached the central regions of g51 since  $z = 0.5$ , the only gas accreted there is characterized by a relatively low metal abundance. For instance, in the *Sal* run of g51 we verified that between  $z = 0.25$  and  $z = 0$  about  $6 \times 10^{12} M_{\odot}$  of gas, having an average metallicity value  $Z_{\text{Fe}} \simeq 0.64 Z_{\text{Fe},\odot}$ , flowed out of  $0.2R_{180}$ . In the same redshift interval, about  $10^{13} M_{\odot}$  of gas was accreted, with an average metallicity  $Z_{\text{Fe}} \simeq 0.42 Z_{\text{Fe},\odot}$ . Therefore, in the absence of large metal-enriched clumps reaching the cluster centre, gas mixing leads to the accretion of relatively metal-poorer gas, thus turning into a decrease of  $Z_{\text{Fe}}$ .

Although the agreement between the runs based on the Salpeter (1955) IMF and observations is rather encouraging, the question remains as to whether the positive evolution seen in the simulations is just the spurious product of the excess of star formation taking place in the central cluster regions. In order to address this question, we compare in the right panel of Fig.2 the evolution



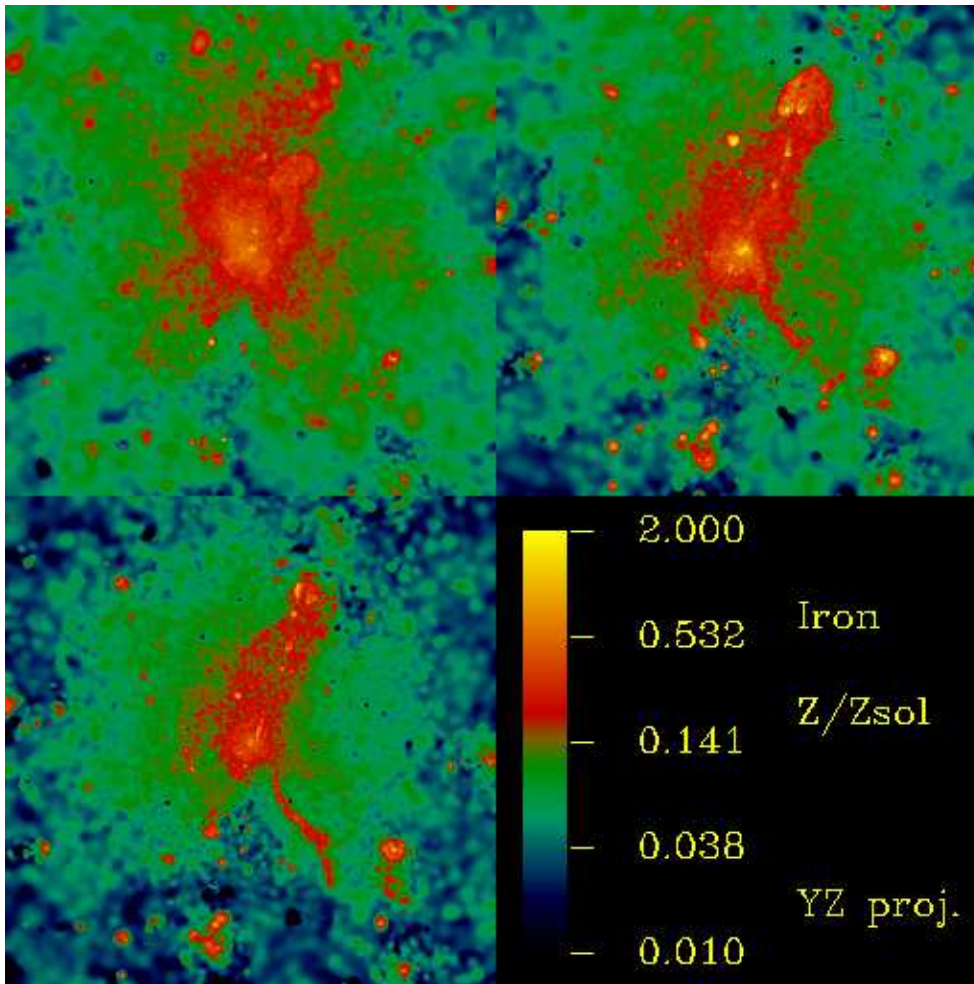


**Figure 3.** Projected maps of the emission-weighted Iron abundance for simulations of the g51 cluster, using the IMF by Salpeter (1955), for the reference run (upper left), for the run with cooling and star formation stopped at  $z = 1$  (CS run; upper right) and for the run in which also the metal production is stopped at  $z = 1$  (CMS run; lower left). Each map is  $2R_{\text{vir}}$  a side.

of  $Z_{\text{Fe}}$  for g51 when stopping star formation and/or metal production at low redshift. Quite remarkably, halting star formation below  $z = 1$  while allowing already formed stars to keep releasing metals (CS run) has the effect of strongly increasing the positive evolution of  $Z_{\text{Fe}}$  in the central region of g51, which turns out to be over-enriched by  $z = 0$ . This leads to the counter-intuitive conclusion that the lack of low- $z$  star formation should generate an increase of the enrichment of the hot gas. In order to investigate the origin of this increase, we show in Figure 3 the emission-weighted metallicity maps of the reference *Sal* run of g51 at  $z = 0$ , along with those of the CS and CMS runs. Quite apparently, the metal distribution in the CS simulation is more clumpy than in the reference run. At the cluster centre, a high  $Z_{\text{Fe}}$  is clearly visible, which boosts the central emission weighted metallicity shown in Fig.2. Indeed, while the emission-weighted  $Z_{\text{Fe}}$  increases by about a factor two within  $0.2R_{180}$ , we verified that the mass-weighted estimate within the same radius increases only by about 10 per cent. In the reference run, the metals released in the high density clumps disappear from the hot diffuse medium due to the efficient gas cooling. As a result, the reference run has a globally higher level of diffuse enrichment, but a lower level of enrichment inside the high-density gas clumps, which dominate the emission-weighted estimate of  $Z_{\text{Fe}}$ . These results demonstrate that the strongly positive evolution of

the emission-weighted metallicity in the CMS run is driven by the accretion of highly enriched dense clumps.

Inhibiting also the production of metals below redshift unity (CMS run) allows us to characterize the role played by gas-dynamical processes in redistributing metals produced at higher redshift. As shown in the bottom-left panel of Fig.3, metal clumps are less pronounced than in the CS run. The global enrichment level of the ICM is now significantly lower than in the reference run, although an enhancement in the innermost regions is still visible. The resulting mass-weighted metallicity within  $0.2R_{180}$  at  $z = 0$  decreases by  $\sim 60$  per cent with respect to the reference run. Therefore, the stability of the emission-weighted metallicity is due to the competing effects of a more clumpy distribution of metals and of a decrease of the overall ICM metal budget.

The maps of Fig.3 also illustrate the role of gas-dynamical effects in redistributing highly enriched gas. Merging clumps within the cluster virial region leave behind them over-enriched tails of stripped gas, which is tempting to explain as due to ram-pressure stripping. However, a significant contribution could well be provided by viscous stripping. Since the SPH scheme is known to be generally characterized by a large numerical viscosity, this may induce an excess of gas stripping from merging halos. Sijacki & Springel (2006b) showed that the effect of including the

Spitzer-Braginskii viscosity in the SPH, on the top of the numerical viscosity, is indeed that of further increasing gas stripping from merging halos. On the other hand, Dolag et al. (2005) discussed an SPH scheme of reduced viscosity. In this case, the increase of the “turbulent” stochastic gas motions should provide a more efficient diffusion of metals from star-forming regions (Rebusco et al. 2005), while making viscous stripping less efficient. Although it is beyond the aim of this paper to carry out an accurate analysis of the effect of viscosity on the pattern of the ICM enrichment, there is no doubt that this aspect deserve an accurate in-depth investigation.

### 3.3 The SnIa rate

The supernova rate represents a useful diagnostic to link the observed evolution of the ICM metallicity to the past history of star formation and to shed light on the relative contribution of SnIa and SnII in releasing metals. In particular the ratio between the Sn rate and the B-band luminosity, the so-called  $\text{Sn}U_B$ , can be used to distinguish the relative contribution of SnIa, which form in binary systems of stars with masses in the range  $(0.8-8) M_\odot$  and the short-living massive stars that contribute substantially to the B-band luminosity of galaxies. In this section we present a comparison between the results of our simulated clusters and observational data of  $\text{Sn}U_B$  in galaxy clusters from Gal-Yam et al. (2002), Mannucci et al. (2008) and Sharon et al. (2007).

The simulation analysis finalized to compute the  $\text{Sn}U_B$  proceeds as follows. For each star particle we know its formation redshift and metallicity. Given the IMF and the lifetime function, this allows us to compute the rate of SnIa exploding in each such particle. Furthermore, using the spectrophotometric GALAXEV code (Bruzual & Charlot 2003) we also compute the B-band luminosity of each star particle, which is treated as a Single Stellar Population (SSP). Once SnIa rates and luminosities are computed for all the star particles, we run the SKID substructure-finding algorithm (Stadel 2001) on their distribution to identify galaxies as gravitationally bound groups of stars. All the star particles not bound to galaxies take part of the intra-cluster diffuse stellar component (e.g., Murante et al. 2007). We refer to Saro et al. (2006) for a detailed description of the procedure to identify galaxies and assign broad-band luminosities to them. In order to reproduce the observational procedure, we compute the  $\text{Sn}U_B$  values by also including the contribution of the SnIa arising from diffuse stars, while the B-band luminosity is computed by including only the contribution of the identified galaxies.

In the left panel of Figure 4 we compare the  $\text{Sn}U_B$  values from the simulations with different IMFs with observational data. In performing this comparison one potential ambiguity arises from the definition of the extraction radius, within which luminosities and SnIa rates are measured in observations, since different authors use different aperture radii. To address this issue we computed  $\text{Sn}U_B$  in the simulations within  $R_{\text{vir}}$  and verified that the results are left unchanged when using instead  $R_{500}$ .

Observational data show a declining trend at low redshift. This is generally interpreted as due to the quenching of recent star formation, which causes the number of SnIa per unit B-band luminosity to decrease after the typical lifetime of the SnIa progenitor has elapsed. On the other hand, our simulations predict a rather flat evolution of the  $\text{Sn}U_B$ , independently of the choice for the IMF, which is the consequence of the excess of low-redshift star formation. The runs based on the Salpeter and on the Kroupa IMF produce very similar results. Although the Kroupa IMF produces a higher rate of SnIa, due to its higher amplitude in the  $(1-8) M_\odot$

stellar mass range, this is compensated by the higher values of  $L_B$ . These two IMFs both agree with the observational data at  $z \gtrsim 0.3$  within the large observational uncertainties, while they overpredict the rates measured for local clusters. Although the excess of recent star formation in the central regions of our simulated clusters produces too blue BCGs (Saro et al. 2006), the large number of SnIa associated to this star-formation overcompensate the excess of blue light.

As for the simulation with the Arimoto-Yoshii IMF, it predicts an even higher  $\text{Sn}U_B$  at low redshift. As shown in the right panel of Fig.4, decreasing the binary fraction to  $A = 0.05$  decreases the value of the  $\text{Sn}U_B$  by more than a factor 2. While this helps in reconciling the simulation results with the low-redshift data, it introduces a tension with the data at  $z \sim 1$ .

Truncating star formation at  $z = 1$  (right panel of Fig.4) has the desired effect of decreasing the value of  $\text{Sn}U_B$  below  $z = 0.5$ . Quite interesting, for  $0.5 \lesssim z \lesssim 1$  the decreasing trend of the SnIa rate is compensated by the corresponding decrease of the B-band luminosity, while it is only at  $z > 0.5$  that the decrease of the SnIa rate takes over causes the decrease of the  $\text{Sn}U_B$  values.

## 4 CONCLUSIONS

We have presented results from cosmological SPH hydrodynamical simulations of galaxy clusters with the purpose of characterising the evolution of the chemical enrichment of the intra-cluster medium (ICM) out to redshift  $z \simeq 1$ . The simulations have been performed with a version of the GADGET-2 code (Springel 2005), which includes a detailed model of chemical evolution (Tornatore et al. 2007). Our simulations have been performed with the purpose of investigating the effect of changing the chemical evolution model and the effect of suppressing star-formation at  $z < 1$ . The main results of our analysis can be summarized as follows.

(a) The Iron abundance profiles provided by simulations based on the Salpeter (1955) IMF are in reasonable agreement with the results from Chandra observations of nearby clusters by Vikhlinin et al. (2005) at  $R \lesssim 0.2R_{500}$ . Simulations based on the IMFs by Kroupa (2001) (*Kr*) and Arimoto & Yoshii (1987) (*AY*) both predict too high a normalization for these profiles. However, reducing the fraction of stars assumed to belong to binary systems suppresses the enrichment level, thus alleviating the disagreement of a top-heavy IMF with the observed  $Z_{\text{Fe}}$  profiles. Our simulations always predict negative metallicity gradients extending out to  $R_{500}$  and beyond, possibly in disagreement with XMM-Newton measurements of the Iron metal abundance at relatively large radii (Snowden et al. 2008).

(b) All our simulations predict a positive evolution of the central Iron abundance, comparable to that observed by Balestra et al. (2007) (see also Maughan et al. 2008). Using a Salpeter IMF also provide an enrichment consistent with observations, while the Kroupa and Arimoto-Yoshii (*AY*) IMFs overpredict the enrichment level at all redshifts. Again, this disagreement can be alleviated by decreasing the fraction of binary systems. It is worth reminding that the observed evolution of the Iron abundance is traced by using a mix of cool-core and non cool-core clusters, while our simulated clusters are all dynamically relaxed. Clearly, a fully self-consistent comparison would require simulating a representative population of clusters, having a variety of morphologies and dynamical states.

(c) Stopping cooling and star formation at  $z = 1$  (CS run) has the

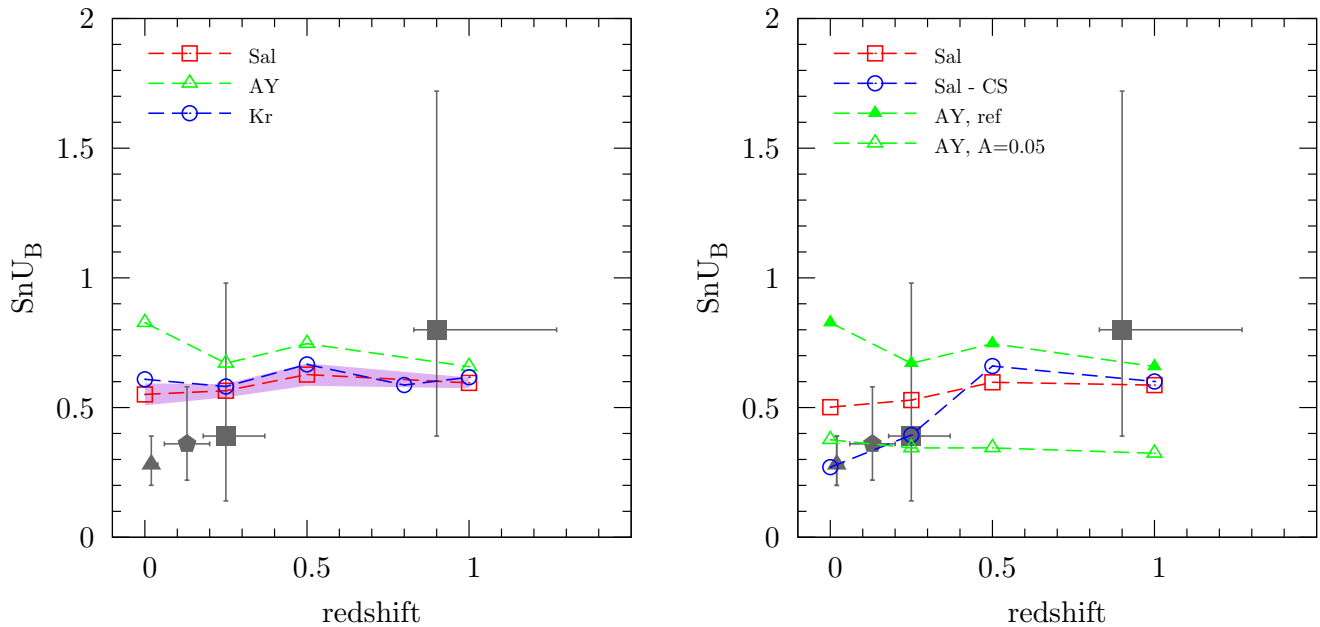


**Figure 4.** Comparison between the observed and the simulated evolution of the SNIa rate per unit B-band luminosity ( $\text{Sn}U_B$ ). In both panels, filled symbols with errorbars refer to observational data from Mannucci et al. (2008) (triangle), Gal-Yam et al. (2002) (squares) and Sharon et al. (2007) (pentagon). Left panel: the effect of changing the IMF. The open squares are for the Salpeter (1955) IMF, the open triangles are for the top-heavy IMF by Arimoto & Yoshii (1987) and the open circles for the IMF by Kroupa (2001). For the Salpeter IMF, the shaded area show the r.m.s. scatter evaluated over the four simulated clusters, while for the other two IMFs only the result for the g51 cluster is shown. Right panel: the effect of suppressing low-redshift star formation and of changing the binary fraction on the  $\text{Sn}U_B$  evolution of the g51 cluster. The open squares and the open circles are for the reference run with Salpeter (1955) IMF and for the same run with cooling and star formation stopped at  $z = 1$  (CS run), respectively. The filled and the open triangles are for the runs with Arimoto & Yoshii (1987) IMF, using  $A = 0.1$  and  $A = 0.05$  for the fraction of binary stars, respectively.

effect of producing a too strong positive evolution of the emission-weighted metallicity. Indeed, in the absence of star formation all the metals released at  $z < 1$  by long-living stars are no longer locked back in the stellar phase. As a result, metallicity is enhanced inside high-density halos and in the central cluster region. The clumpy metal distribution boosts the emission-weighted abundance estimate. This leads to the somewhat counter-intuitive conclusion that suppressing recent star formation has the effect of enhancing the positive evolution of the ICM metallicity.

(d) A comparison of the SNIa rate per unit B-band luminosity,  $\text{Sn}U_B$ , show that our simulations are generally not able to reproduce the observed declining trend at low redshift. This result is explained by the excess of recent star formation taking place in the central regions of galaxy clusters. Indeed, excising star formation at  $z < 1$  produces an evolution of  $\text{Sn}U_B$  which is consistent with the observed one.

Cluster simulations which only include stellar feedback, like those presented here, are well known to be at variance with a number of observations, such as the temperature profiles in the cool core regions and an large excess of recent star formation in the BCG. Our prescription to quench recent star formation is admittedly oversimplified. A more realistic treatment would require introducing energy feedback from gas accretion onto super-massive black holes, which self-consistently follow the hierarchical build-up of the cluster (e.g., Sijacki & Springel 2006a). Still, our results highlight that the positive evolution of the metal abundance in the central regions of simulated clusters can not be simply interpreted as a consequence of an excess of low-redshift star formation. In

fact, the evolution of the metallicity pattern is driven by the combined action of the gas-dynamical processes, which redistribute already enriched gas, and of star formation, which acts both as a source and as a sink of metals. While hydrodynamical simulations probably provide the most complete interpretative framework for observations of the history of the ICM enrichment, they have still to improve in the numerical accuracy for the description of relevant physical processes. There is no doubt that the ever increasing super-computing power and efficiency of simulation codes should be paralleled by a comparable advance in the reliability of the numerical description of the relevant astrophysical and gas-dynamical processes. Only in this way, simulations will become the standard tool to link ICM observations to the global picture of cosmic structure formation.

#### ACKNOWLEDGMENTS

We are greatly indebted to Volker Springel for having provided us with the non-public version of GADGET-2. We thank Silvia Ameglio for her help in producing the metallicity maps of Fig.3, and Alexey Vikhlinin for having provided the data points shown in Fig.1. We acknowledge useful discussions with Francesco Calura, Stefano Ettori, Alexis Finoguenov, Pasquale Mazzotta, Pierluigi Monaco, Elena Rasia and Paolo Tozzi. The simulations have been carried out at the “Centro Interuniversitario del Nord-Est per il Calcolo Elettronico” (CINECA, Bologna), with CPU time assigned thanks to an INAF-CINECA grant and to an agreement between CINECA and the University of Trieste, and on the Linux Clusters



at INAF in Catania and at the University of Trieste. This work has been partially supported by the INFN PD-51 grant, by the INAF-PRIN06 Grant and by a ASI-AAE Theory grant.

**REFERENCES**

Arimoto N., Yoshii Y., 1987, *A&A*, 173, 23  
 Balestra I., Tozzi P., Ettori S., Rosati P., Borgani S., Norman V. M. C., Viola M., 2007, *A&A*, 462, 429  
 Baumgartner W. H., Loewenstein M., Horner D. J., Mushotzky R. F., 2005, *ApJ*, 620, 680  
 Bhattacharya S., Di Matteo T., Kosowsky A., 2007, *ArXiv e-prints*, 710  
 Böhringer H., Matsushita K., Churazov E., Finoguenov A., Ikebe Y., 2004, *A&A*, 416, L21  
 Borgani S., Fabjan D., Tornatore L., Schindler S., Dolag K., Diaferio A., 2008, *ArXiv e-prints*, 801  
 Bruzual G., Charlot S., 2003, *MNRAS*, 344, 1000  
 Calura F., Matteucci F., Tozzi P., 2007, *MNRAS*, pp L43+  
 Chung A., van Gorkom J. H., Kenney J. D. P., Vollmer B., 2007, *ApJ*, 659, L115  
 Cora S. A., Tornatore L., Tozzi P., Dolag K., 2008, *ArXiv e-prints*, 802  
 De Grandi S., Ettori S., Longhetti M., Molendi S., 2004, *A&A*, 419, 7  
 Dolag K., Vazza F., Brunetti G., Tormen G., 2005, *MNRAS*, 364, 753  
 Domainko W., Mair M., Kapferer W., van Kampen E., Kronberger T., Schindler S., Kimeswenger S., Ruffert M., Mangete O. E., 2006, *A&A*, 452, 795  
 Ettori S., 2005, *MNRAS*, 362, 110  
 Gal-Yam A., Maoz D., Sharon K., 2002, *MNRAS*, 332, 37  
 Greggio L., Renzini A., 1983, *A&A*, 118, 217  
 Grevesse N., Sauval A. J., 1998, *Space Science Reviews*, 85, 161  
 Haardt F., Madau P., 1996, *ApJ*, 461, 20  
 Kroupa P., 2001, *MNRAS*, 322, 231  
 Loewenstein M., 2006, *ApJ*, 648, 230  
 Mannucci F., Maoz D., Sharon K., Botticella M. T., Della Valle M., Gal-Yam A., Panagia N., 2008, *MNRAS*, 383, 1121  
 Matteucci F., Gibson B. K., 1995, *A&A*, 304, 11  
 Matteucci F., Greggio L., 1986, *A&A*, 154, 279  
 Maughan B. J., Jones C., Forman W., Van Speybroeck L., 2008, *ApJS*, 174, 117  
 Mazzotta P., Rasia E., Moscardini L., Tormen G., 2004, *MNRAS*, 354, 10  
 Murante G., Giovalli M., Gerhard O., Arnaboldi M., Borgani S., Dolag K., 2007, *MNRAS*, 377, 2  
 Mushotzky R. F., 2004, in *Mulchaey J. S., Dressler A., Oemler A., eds, Clusters of Galaxies: Probes of Cosmological Structure and Galaxy Evolution Clusters of Galaxies: An X-ray Perspective.* pp 123+  
 Padovani P., Matteucci F., 1993, *ApJ*, 416, 26  
 Portinari L., Moretti A., Chiosi C., Sommer-Larsen J., 2004, *ApJ*, 604, 579  
 Rafferty D. A., McNamara B. R., Nulsen P. E. J., Wise M. W., 2006, *ApJ*, 652, 216  
 Rasia E., Mazzotta P., Bourdin H., Borgani S., Tornatore L., Ettori S., Dolag K., Moscardini L., 2007, *ArXiv e-prints*, 707  
 Rasmussen J., Ponman T. J., 2007, *MNRAS*, 380, 1554  
 Rebusco P., Churazov E., Böhringer H., Forman W., 2005, *MNRAS*, 359, 1041  
 Renzini A., 1997, *ApJ*, 488, 35  
 Renzini A., 2004, in *Mulchaey J. S., Dressler A., Oemler A., eds, Clusters of Galaxies: Probes of Cosmological Structure and Galaxy Evolution The Chemistry of Galaxy Clusters.* pp 260+  
 Roediger E., Brügggen M., 2007, *MNRAS*, 380, 1399  
 Roediger E., Brügggen M., Rebusco P., Böhringer H., Churazov E., 2007, *MNRAS*, 375, 15  
 Romeo A. D., Portinari L., Sommer-Larsen J., 2005, *MNRAS*, 361, 983  
 Romeo A. D., Sommer-Larsen J., Portinari L., Antonuccio-Delogu V., 2006, *MNRAS*, 371, 548  
 Salpeter E. E., 1955, *ApJ*, 121, 161  
 Saro A., Borgani S., Tornatore L., Dolag K., Murante G., Biviano A., Calura F., Charlot S., 2006, *MNRAS*, 373, 397  
 Sharon K., Gal-Yam A., Maoz D., Filippenko A. V., Guhathakurta P., 2007, *ApJ*, 660, 1165  
 Sijacki D., Springel V., 2006a, *MNRAS*, 366, 397  
 Sijacki D., Springel V., 2006b, *MNRAS*, 371, 1025  
 Snowden S. L., Mushotzky R. F., Kuntz K. D., Davis D. S., 2008, *A&A*, 478, 615  
 Springel V., 2005, *MNRAS*, 364, 1105  
 Springel V., Hernquist L., 2003, *MNRAS*, 339, 289  
 Springel V., Yoshida N., White S., 2001, *New Astronomy*, 6, 79  
 Stadel J. G., 2001, *Ph.D. Thesis*  
 Sutherland R. S., Dopita M. A., 1993, *ApJS*, 88, 253  
 Thielemann F.-K., Argast D., Brachwitz F., Hix W. R., Höflich P., Liebendörfer M., Martinez-Pinedo G., Mezzacappa A., Panov I., Rauscher T., 2003, *Nuclear Physics A*, 718, 139  
 Tormen G., Bouchet F., White S., 1997, *MNRAS*, 286, 865  
 Tornatore L., Borgani S., Dolag K., Matteucci F., 2007, *MNRAS*, 382, 1050  
 Tornatore L., Borgani S., Matteucci F., Recchi S., Tozzi P., 2004, *MNRAS*, 349, L19  
 Valdarnini R., 2003, *MNRAS*, 339, 1117  
 van den Hoek L. B., Groenewegen M. A. T., 1997, *A&AS*, 123, 305  
 Vikhlinin A., Markevitch M., Murray S. S., Jones C., Forman W., Van Speybroeck L., 2005, *ApJ*, 628, 655  
 Werner N., Durret F., Ohashi T., Schindler S., Wiersma R. P. C., 2008, *ArXiv e-prints*, 801  
 Woosley S. E., Weaver T. A., 1995, *ApJS*, 101, 181  
 Yoshida N., Sheth R. K., Diaferio A., 2001, *MNRAS*, 328, 669